Evaluation of Perfect and Imperfect-Gas Interferograms by Computer

G. Ben-Dor,† B. T. Whitten, ‡ and I. I. Glass§

A digital method of evaluating interferograms was developed in order to extract the maximum amount of information from interferograms of complex-flow phenomena in shock tubes such as ionizing-gas shock structures and their induced laminar boundary layers as well as real-gas nonstationary oblique-shock-wave diffractions. The method is based on a new approach to the interpretation of interferograms. In this approach the spatial coordinates (x, y) of the various lines of interference (fringes) on the interferogram are put into digital form, thereby readily making computer analysis possible. The new method is not only many times faster but it also removes most of the painstaking drudgery from evaluating interferograms and provides for greater accuracy and insight.

NOTATION

- a entrance position to test section
- Ar argon atom
- A_r^+ argon ion
- b exit position from test section
- c_0 speed of light in vacuum
- e electron charge
- k arbitrary constant
- K Gladstone–Dale constant
- K_A atomic Gladstone–Dale constant
- K_I ion Gladstone–Dale constant
- K_M molecular Gladstone–Dale constant
- l geometrical length travelled by light
- L geometrical distance across test section
- m isopycnic number
- m_e electron mass
- M continuous fringe number
- M' integer fringe number
- M_s incident shock wave Mach number
- n index of refraction
- n_e electron number density
- N continuous variable
- N' integer variable
- N_2 nitrogen molecule
- P pressure
- S fringe shift
- t time
- T temperature
- x spatial coordinate
- X collision partner
- y spatial coordinate
- z spatial coordinate
- α degree of dissociation
- δ first variation of an integral
- $\Delta\beta$ change in property β
- ε angle of rotation of second beam splitter in interferometer
- θ_w wedge angle
- λ light source wavelength
- λ_0 light source wavelength in vacuum
- ρ density
- τ optical path length
- τ^* optical path length inside the test section
- ω light source frequency
- ω_p plasma frequency
- χ degree of ionization

Subscripts

- E ionization equilibrium conditions
- p test section arm
- q compensation chamber arm
- r reference point
- 0 'no-flow' conditions

1 INTRODUCTION

Optical techniques possess several distinct advantages for flow investigation. For practical purposes they are free from inertia lag; they do not require the introduction of a disturbing mechanical probe into the flow field, and they record conditions throughout an extended area of the flow field rather than conditions at one point. Of the three techniques—shadowgraph, schlieren, and interferometry—all useful and complementary for gas-flow studies, interferometry is the most important for obtaining quantitative information about density fields. Interferograms of two-dimensional or rotationally-symmetric flows may be evaluated to obtain density variations throughout the entire field. For these reasons the interferometer has been used as a major experimental instrument in studying different flow phenomena such as subsonic, transonic, supersonic, and hypersonic flows, boundary layers, natural (free) convection heat transfer, and other applications.

At low and moderate temperatures, when dissociation and ionization are negligible, a relatively simple expression relates the density ρ to the refractive index n **(1)**,

$$n - 1 = K\rho \tag{1.1}$$

where K is the Gladstone–Dale constant of the gas under consideration. If a mixture of gases is investigated, eq. (1) becomes **(2)**

$$n - 1 = \sum_i K_i \rho_i \tag{1.1a}$$

where ρ_i is the partial density of the ith species and K_i is the corresponding Gladstone–Dale constant. Con-

† Now, Lecturer, Department of Mechanical Engineering, Ben-Gurion University of the Negev, Beer Sheva, Israel.
‡ Now, Defence Scientist, Defence Research Establishment Atlantic, Dartmouth, Nova Scotia, Canada.
§ Institute for Aerospace Studies, University of Toronto, Toronto, Ontario, Canada M3H 5T6.
Received on 2 December 1978 and accepted for publication on 6 April 1979.

0142-727X/79/0600-0077$02.00

sequently, if a dissociated diatomic gas (e.g., $N_2 + X \rightleftarrows 2N + X$) is considered as a gas mixture of molecules (N_2) and atoms (N) eq. (1.1a) yields (**2**),

$$n - 1 = \rho[K_M(1 - \alpha) + K_A\alpha] \qquad (1.1b)$$

where K_M and K_A are the molecular and atomic Gladstone–Dale constants, respectively, and α is the degree of dissociation. For a singly-ionized gas (e.g., $Ar + X \rightleftarrows Ar^+ + e + X$) eq. (1.1a) results in (**3**)

$$n - 1 = \rho[K_A(1 - \chi) + K_I\chi] - \frac{\omega_p^2}{2\omega^2} \qquad (1.1c)$$

where K_A and K_I are the Gladstone–Dale constants of the atom and the ion, respectively, χ is the degree of ionization, ω and ω_p are the light source and the plasma frequencies, respectively, given by (**3**)

$$\omega = 2\pi\nu = 2\pi\frac{c_0}{\lambda_0}, \qquad \omega_p = \left(\frac{4\pi n_e e^2}{m_e}\right)^{1/2}$$

Note from eq. (1.1c) that the contribution of the electrons to the index of refraction is opposite to that of the atoms or ions. Inserting the appropriate values into the above expression for ω and ω_p finally results in, for a singly ionized plasma (**3**):

$$n - 1 = \rho[K_A(1 - \chi) + K_I\chi] - 4{\cdot}46 \times 10^{-4}\lambda_0^2 n_e \qquad (1.1d)$$

The Gladstone–Dale constant depends on the light-source wavelength and the nature of the gas, and to a large extent it is independent of the pressure of the gas.

In most applications to gas dynamics one wants to know the density at a definite position in space. For this purpose it is normally required that the fringes be located at this point in order to obtain the appropriate interferogram needed for the evaluation (**1**).

The Mach–Zehnder arrangement of the interferometer which has the ability of locating fringes at any desired place by suitably rotating its mirrors and/or beam-splitters, is very suitable for this purpose. The Mach–Zehnder interferometer was developed by Zehnder (**4**) and Mach (**5**) in the early 1890s. It uses a beam-splitter and plane mirror to divide light from one source into two coherent and parallel beams. One of the coherent beams is passed through the gas flow being studied, while the other serves as a fixed reference arm. A second beamsplitter and mirror combination reunites the two coherent beams to produce interference fringes. For relatively large-scale technical applications in wind-tunnel or shock-tube studies, the Mach–Zehnder arrangement has proved to be most practical. The fact that the flow under study is traversed only once by the test beam (unlike the Michelson arrangement) renders interpretation of the interferograms relatively straightforward. Detailed reviews and discussions of the theoretical aspects involved with the Mach–Zehnder interferometer as well as its history and construction can be found in references (**1**), (**6**), (**7**), (**8**), and (**16**).

The interferometer measures the refractive index; consequently it is possible to obtain its value at any point in a given interferogram (**1**). Thus in the case of a non-dissociating or non-ionizing gas eq. (1.1) can be used to determine the density. In the case of dissociating or ionizing gases the refractive index is related additionally to the degree of dissociation or ionization (eqs. (1.1b) and (1.1c)). Therefore, two simultaneous interferograms with two different wavelengths are necessary in order to provide an additional relation. This is usually done today by using a laser with a second harmonic (wavelength) generator as a light source.

It is clear from the above discussion that the major task in evaluating interferograms is to determine the refractive index at any desired point. Unfortunately, the well-known simple and direct method (**1**), (**8**) of deducing the refractive index from the corresponding interferograms is inefficient and inaccurate as the flow under consideration becomes complex. Such examples taken in the 10 cm × 18 cm Hypervelocity Shock Tube at the Institute for Aerospace Studies are shown in Figs. 1(a) and (b). Interferograms such as these, with their dark and bright lines of interference, or fringes, contain a vast amount of information about the refractive index variations over the entire field of view. In order to extract the maximum amount of data in complex flows a digital evaluation method was employed. For this technique a new approach to the interpretation of interferograms was developed. In this approach the spatial coordinates (x, y) of the various lines of interference (fringes) on the interferograms are put into digital form, thereby making a computer analysis possible.

2 ANALYSIS

In developing the relationships between orders of interference and refractive index, the basics of interferometry are reviewed briefly as applied to the Mach–Zehnder interferometer whose components are shown in Fig. 2. (More details may be found in references (**1**), (**8**), and (**16**).) Light from a coherent monochromatic source is divided by a first beam splitter S_1, into two coherent beams, one of which travels through the test section p, while the other travels through a compensation chamber q. When reunited at the second splitter, S_2, the light waves will interfere constructively or destructively depending on the relative time of travel through each arm. The time taken for a plane electromagnetic wave to pass through an isotropic medium may be written in terms of the 'optical path length' τ as

$$\Delta t = \frac{1}{c_0}\tau$$

where c_0 is the speed of light in vacuo, and

$$\tau = \int n\,\mathrm{d}l$$

where n is the refractive index, which is a function of the medium and of the frequency of the wave, and l is the geometrical path over which the wave travels, or the arc length. For coherent light, constructive interference occurs if the difference in optical path lengths between the two arms is an even multiple of half wavelengths of the light used, while destructive interference takes place if this difference is an odd multiple, that is,

$$\int_{S_1}^{S_2} n_p\,\mathrm{d}l_p - \int_{S_1}^{S_2} n_q\,\mathrm{d}l_q = \begin{cases} 2N'(\lambda/2) & \text{for maxima} \\ (2N' + 1)(\lambda/2) & \text{for minima} \end{cases} \qquad (2.1)$$

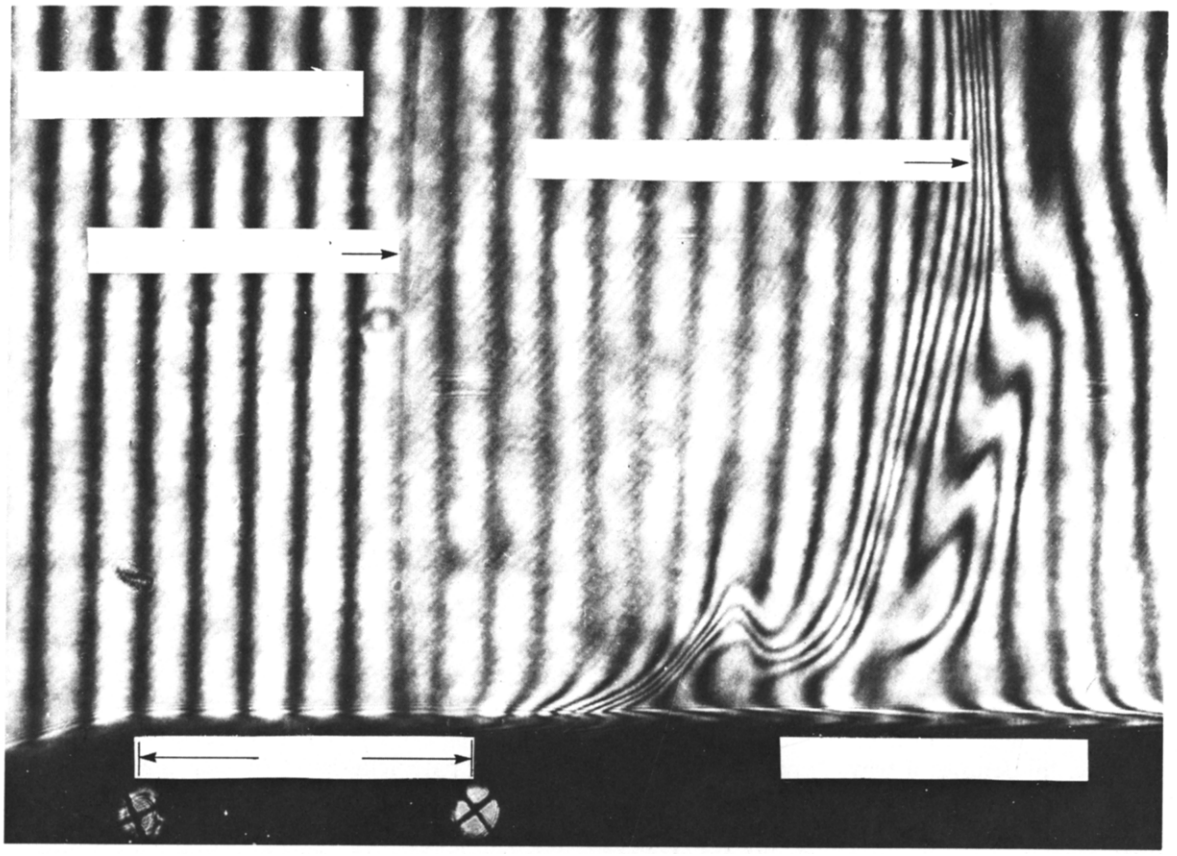

Fig. 1(a). Interferogram of non-stationary shock wave structure in argon near the shock-tube wall (distance between reference cross-wires is 1 cm). Incident shock wave Mach number $M_s = 15{\cdot}9$, light source wavelength $\lambda = 6943$ Å (shock wave is travelling from right to left)

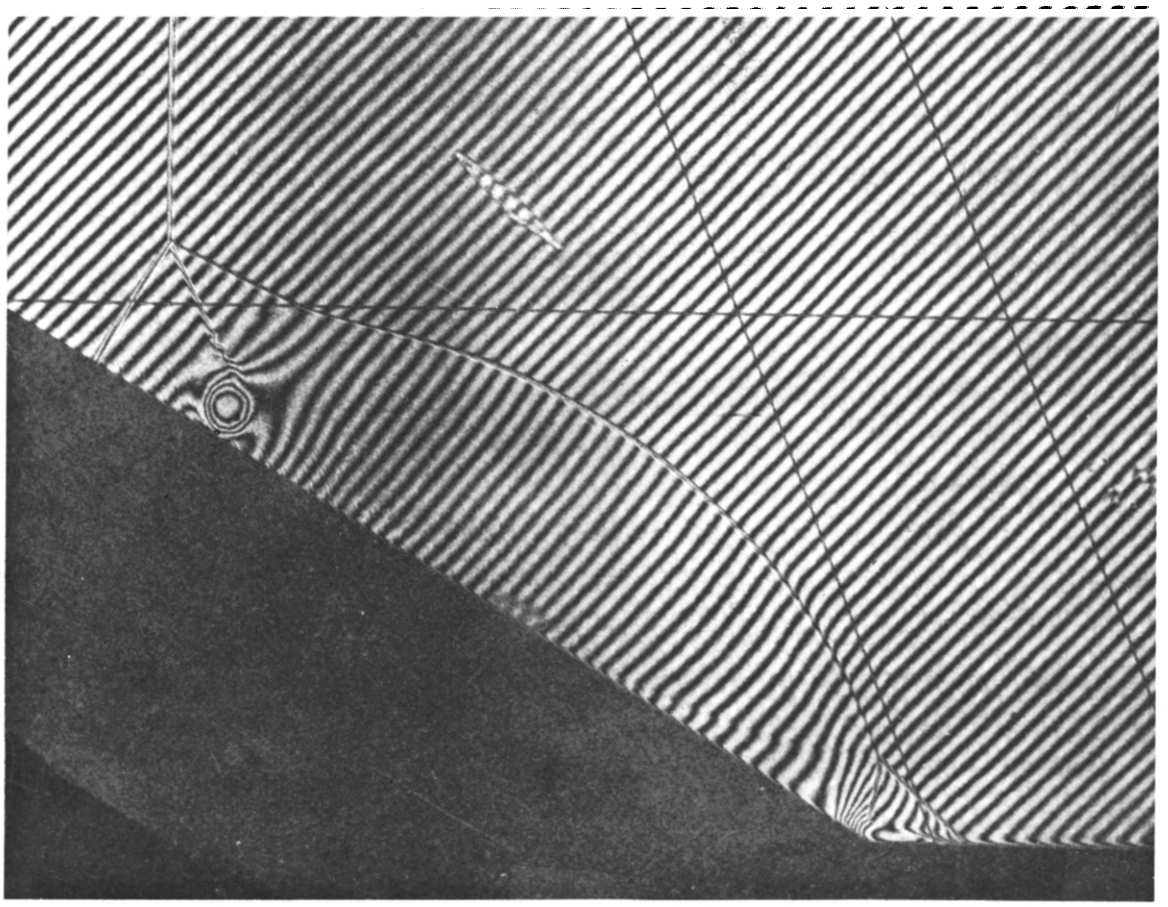

Fig. 1(b). Interferogram of a non-stationary double-Mach reflection in nitrogen produced by a sharp compressive wedge of angle $\theta_w = 20°$ at an initial Mach number $M_s = 6{\cdot}27$, initial pressure and temperature of $P_0 = 15{\cdot}33$ torr, $T_0 = 296{\cdot}0$ K and light source wavelength $\lambda = 3471{\cdot}5$ Å (shock wave is travelling from right to left)

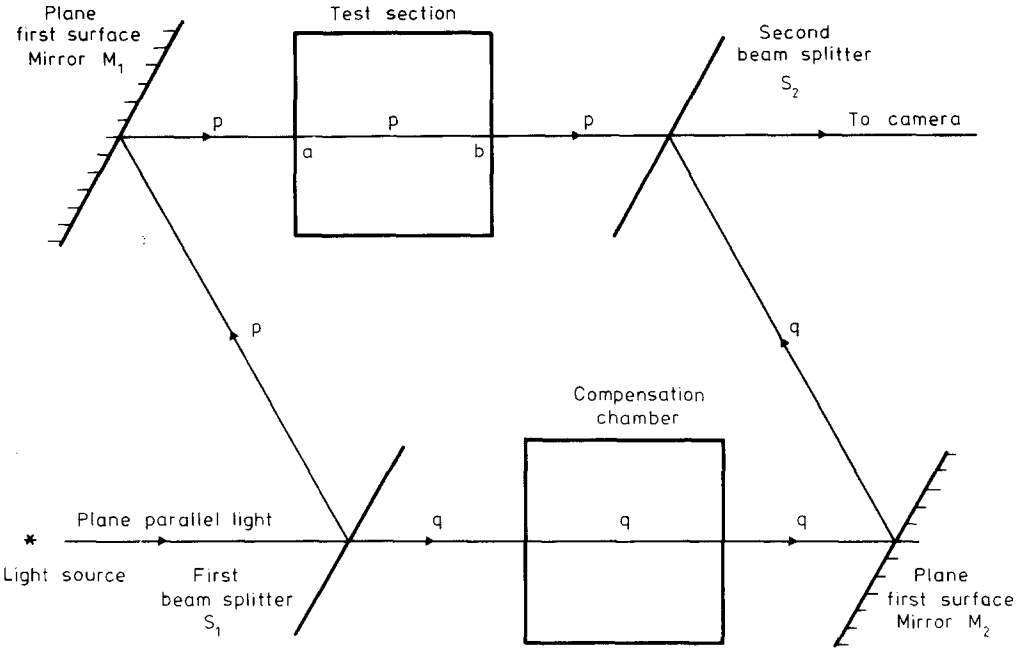

Fig. 2. Basic components of a Mach–Zehnder interferometer

where $N' = 0, \pm 1, \pm 2, \ldots$ may be termed the order of the interference, 'p' denotes a wave travelling through the test section arm and 'q' denotes a wave travelling through the compensation arm. For convenience, let the optical path lengths in the respective arms be denoted as

$$\tau_q = \int_{S_1}^{S_2} n_q \, dl_q$$

$$\tau_p = \int_{S_1}^{S_2} n_p \, dl_p = \int_{S_1}^{a} n_p \, dl_p + \int_{a}^{b} n_p \, dl_p + \int_{b}^{S_2} n_p \, dl_p$$

Here, the optical path length through the test section has been broken at 'a', the entrance position to the test section, and 'b', the exit position from the test section, into three additive components. The term τ^*, is then defined as:

$$\tau^* = \int_{S_1}^{a} n_p \, dl_p + \int_{b}^{S_2} n_p \, dl_p - \tau_q \qquad (2.2)$$

such that τ^* accounts for *all* the optical path lengths outside the test section. The interference eq. (2.1) may then be written as

$$\int_a^b n_p \, dl_p + \tau^* = \begin{cases} 2N'(\lambda/2) & \text{for maxima} \\ (2N'+1)(\lambda/2) & \text{for minima} \end{cases}$$

To write an easier and more general relationship, a continuous linear variable, N, is considered such that:

$$\int_a^b n_p \, dl_p + \tau^* = N\lambda \qquad (2.3)$$

where, for $N = 0, \pm 1, \pm 2, \ldots$, there will be total constructive interference, or maxima; while for $N = \pm 1/2, \pm 3/2, \pm 5/2, \ldots$, there will be total destructive interference, or minima. For all other intermediate values of N, there will be varying 'grey' interference, or a gradation of these two extremes.

The quantity of interest is generally the refractive index n_p of the medium in the test section, which is then related to the density. Thus, if the path taken by the light travelling through the test section is known, and all the optical path lengths τ^* outside the test section are accounted for, then orders of interference N measured from an interferogram may be used with eq. (2.3) to determine the integrated or cumulative value of n_p over this path. To determine τ^* for this equation, the interference may be observed for a case where the optical path lengths in the test section are known (e.g., n_p = constant). This picture is referred to as the 'no-flow' or reference interferogram, and is denoted by the subscript 0. Then

$$\tau_0^* = N_0\lambda - \int_a^b n_{p_0} \, dl_{p_0}$$

where

$$\int_a^b n_{p_0} \, dl_{p_0}$$

is known, and N_0 is measured from the no-flow interferogram.

After the event being studied in the test section is recorded by the 'flow' interferogram, τ_0^* may be used in eq. (2.3) to find n_p, providing no changes have occurred in the optical path lengths outside the test section (i.e., $\tau^* = \tau_0^*$). However, this assumption is often subject to uncertainty, particularly if the time between the recording of the 'no-flow' and 'flow' interferograms is significant. A less stringent dependence on the no-flow picture can be invoked by the use of a 'reference point' in the flow interferograms as described later.

Consider the coordinate system shown in Fig. 3 where the light propagation is initially in the z-direction. In the most general case, the refractive index may vary over the entire field, such that $n = n(x, y, z)$. The light path must also be such that the travel time be a minimum as given by Fermat's principle,

$$\delta\left[\frac{1}{c_0}\int n(x, y, z)\, dl\right] = 0$$

where δ denotes the first variation of the integral.

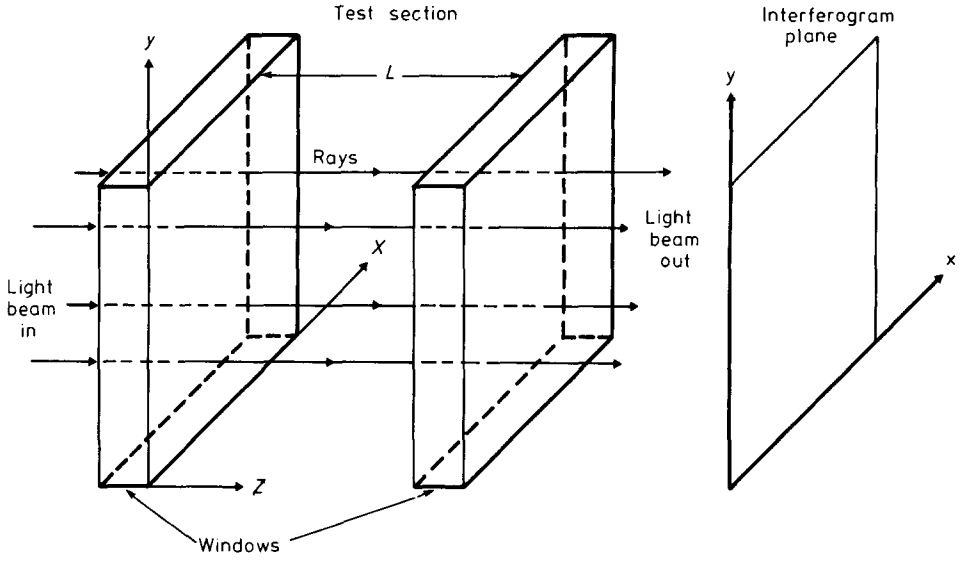

Fig. 3. Coordinate system used for interferometric analysis

However, to keep the analysis from becoming too cumbersome, the following assumptions are made for a first-order approximation:

(1) To satisfy Fermat's principle, the refraction of light is small such that each beam may be considered to travel in a straight line path in the z-direction, perpendicular to the (x, y)-plane.
(2) The refractive index n varies only across the field of view or in the (x, y)-plane, and does not vary along the beam direction z.
(3) The test section windows enclosing the test chamber are exactly parallel, such that, for any (x, y)-value, the geometrical distance across the test section in the z-direction is the same value L.

The first assumption is satisfactory for many flows being examined, but becomes questionable in regions where density gradients are high. The second merely emphasizes that the interferometer is most convenient in analysing two-dimensional flows, and becomes much more difficult to use quantitatively if changes occur in the beam direction because of the integrated effect. The third assumption is usually good, and may be precontrolled to a known accuracy in the equipment.

Mathematically, the above stipulations translate into eq. (2.3) in the following manner:

(1) $\mathrm{d}l_p = \mathrm{d}z$
(2) $n_p = n_p(x, y)$, $\tau^* = \tau^*(x, y)$
(3) $b - a = L$ for all (x, y)

Hence,

$$\int_a^b n_p \, \mathrm{d}l_p = n(x, y)L$$

and

$$n(x, y)L + \tau^*(x, y) = N(x, y)\lambda \qquad (2.4)$$

Note that the order of interference N may vary across the field of view or become a function of (x, y) if the optical path lengths outside the test section and the refractive index inside the test section vary across (x, y). Equation (2.4) makes it possible to have a digital analysis.

Some useful comments concerning the adjustment of a Mach–Zehnder interferometer will be made. In the 'ideal' case with perfect optical components and coherent light, it would be possible to adjust the interferometer perfectly such that the optical lengths outside the test section do not vary over the (x, y)-plane or field of view, such that τ^* is constant, and not a function of (x, y). Then, with constant conditions in the test section, there would be a constant interference across the (x, y)-field and hence a uniform illumination over the entire viewing screen. In other words, the screen would be totally bright, dark or gray. This adjustment leads to what is termed the 'infinite fringe' method (i.e., the fringes are spaced infinitely far apart).

When changes take place in the test section during a flow, any fringes, or lines of extreme interference, which are visible will just correspond to lines of constant refractive index. This follows immediately from eq. (2.4).

$$n(x, y)L + \tau^* = N(x, y)\lambda$$

Since τ^* = constant, the orders of interference, $N(x, y)$, which are seen on the screen are directly related to the refractive index, $n(x, y)$. Along any fringe, $N(x, y) =$ constant, and therefore $n(x, y)$ must be a constant. This method is often used for a qualitative examination of a flow, particularly in cases where the refractive index can be directly related to the density of the medium, as in a perfect gas. Any fringes which are visible are isopycnics or lines of constant density. However, the fringes are usually quite wide and accuracy is therefore impaired. Consequently, the infinite-fringe method is poor for quantitative measurements that require very good spatial resolution of density.

Since only the extreme lines of interference (fringes) are easily detected from interferograms, the refractive index and hence density must change a sufficient amount through the flow to cause changes in optical path lengths equivalent to *integer* changes of wavelength. Otherwise, perhaps only one or two fringes will be visible over the entire flow from which to determine the results. In other

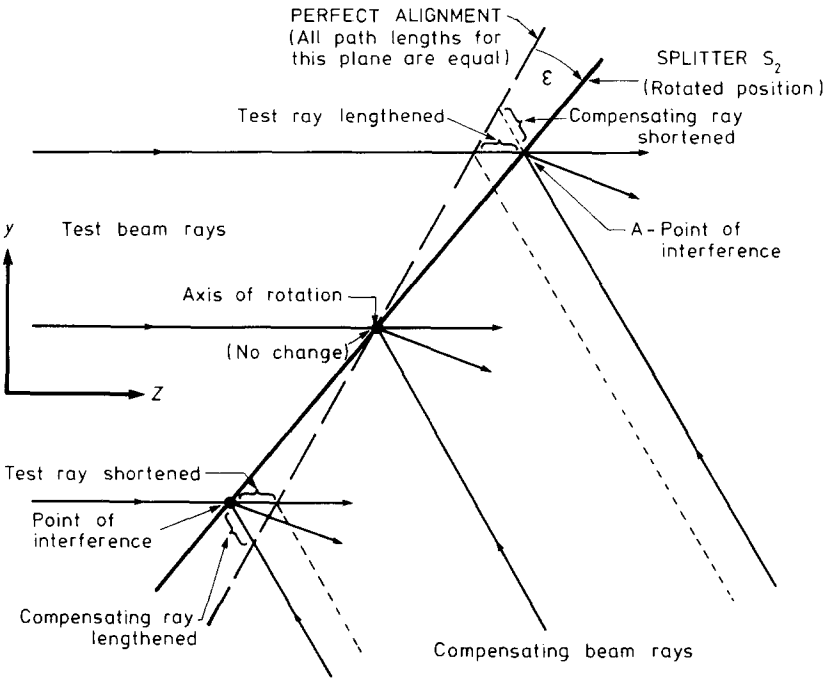

Fig. 4. 'Virtual' fringe created in the plane of splitter S_2

words, the spatial resolution is generally poor. This also makes it difficult to determine the *exact* order of interference along the visible fringe, which is necessary in calculating the refractive index. Finally, it is almost impossible to obtain the perfect optical components to provide uniform interference over a very large area. Consequently, a fringe or two may appear only because of optical imperfections, and this effect may be difficult to account for.

These problems are overcome by using the *'virtual fringe'* method. In this case, one or more of the components of the interferometer are rotated slightly to produce geometrical path differences between the test section and compensating beams *outside* the test section. The basics of this technique are shown in Fig. 4, in which the clockwise rotation of splitter S_2 by an angle ε about the x-axis, produces different distances in the light path directions to where the interfering beams reunite. For positions (y, z) on the splitter above the axis of rotation, the path lengths of the test section arm are increased while those of the compensation arm are shortened, and below the axis, the opposite is true. Looking over the (x, y)-field of view, as y increases, the path lengths in the test section arm continuously increase linearly while those in the compensation arm continuously decrease, independent of x. Therefore, with constant conditions in the test section, horizontal lines of extreme interference will appear, each successive fringe occurring at a value of y where the path length *difference* is again such as to produce the next minimum or maximum as shown on actual interferograms in Fig. 5. As the angle ε increases, the path-length changes in the y-direction become more severe and the spacing between the fringes becomes smaller. Each successive fringe in the y-direction corresponds to the next higher order of interference, since the test section path lengths increase as y increases. Had the rotation of S_2 been in a counter-clockwise direction, the changes as a function of y would be reversed and horizontal fringes would again appear, although the orders of interference would not decrease in the y-direction. Although this very simplified description of fringe formation omits the details of focusing (7), it should suffice for this analysis.

With available controlled rotation of the optical components about both the x and y-axes, the spacing and orientation of these 'virtual' fringes can be chosen for the optimum spatial resolution of the flow being studied. The more fringes that are in the region of interest, the more locations are known at which there is identifiable interference. Consider one such location (x, y) where there is, for example, after adjustment of the interferometer, a maximum corresponding to a particular integer order of interference N'. If the refractive index in the test section then changes in the region of (x, y), the optical path lengths will change altering the order of interference, and there will no longer be a maximum at this location. The maximum corresponding to N' will now be at some new location where the new optical path length inside the test section and the appropriate path difference outside again cause the same constructive interference. It is the measurement from an interferogram of fractional changes in fringe position which permits a sensitive determination of changes in refractive index and hence density.

In an interferogram such as Fig. 1, the lines of constant extreme interference, or fringes, along which there is total constructive or destructive interference, are easily identified. For example, each bright line corresponds to a maximum, where $N(x, y) = N'$, and N' is some integer along the line. Although the exact integer value N', may not be known, the fringe can be assigned an arbitrary 'fringe number' M'. The next bright line of interference will generally correspond to an integer value of either $N' + 1$ or $N' - 1$, depending on the direction of rotation in the initial virtual fringe adjustment. In other words, between consecutive bright fringes (or between consecu-

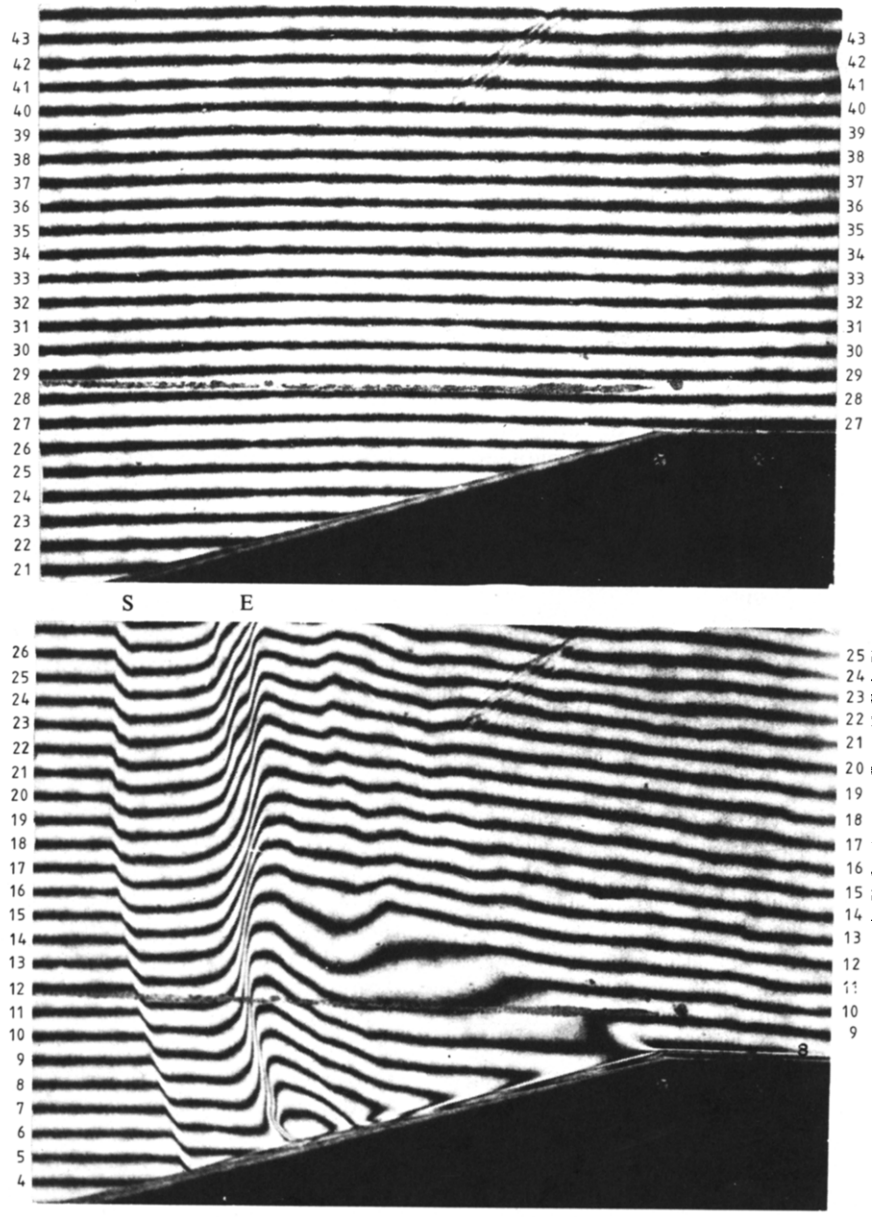

Fig. 5. Diffraction around an expansion corner of an ionizing shock wave in argon (shock wave is travelling from right to left), S—translational shock front, E—electron cascade front, SE—ionization relaxation distance

(a) no-flow interferogram ($\lambda = 6943$ Å)
(b) flow-interferogram ($\lambda = 6943$ Å)

tive dark fringes), $\Delta N' = \pm 1$. Hence, if this next fringe is assigned a fringe number, $M' + 1$, such that $\Delta M' = 1$, there will be a linear relationship established between the assigned fringe numbers M', and the actual interference orders N'. In mathematical terms, if

$$\Delta N' = \pm \Delta M',$$

then

$$N' = \pm M' + k, \text{ where } k = \text{constant}$$

If the fringes have been given increasing numbers in the same direction as the actual orders of interference increase, then the plus sign prevails, while if the numbering were done in the opposite direction, the minus sign must be used. If each fringe has been assigned an integer fringe number correctly relative to the others, there will be the same difference k between the true orders of interference and the assigned fringe numbers over the entire interferogram. Thus, the fringe numbers will represent the actual orders of interference to within the unknown constant k. It should be pointed out at this stage that the major problem in analysing complex flows from interferograms is, in fact, the correct assignment of fringe numbers over the field to represent the interference correctly. Often, fringes become difficult to follow, and extreme care must be taken. This aspect will be discussed later.

The fringe number M' may be generalized to a continuous linear variable M, as was done for the interference order N, in eq. (2.3). In this case, the centre of a fringe is taken as the location where M has the integral value of the fringe number. This corresponds to the assumption that the position of extreme interference (either total constructive or total destructive) is at the centre of the observed brightness or darkness. Then

$$N(x, y) = \pm M(x, y) + k$$

Substituting into eq. (2.4) yields

$$n(x, y)L + \tau^*(x, y) = \pm M(x, y)\lambda + k\lambda \qquad (2.6)$$

From any interferogram, $M(x, y)$ can be determined after numbering each successive fringe correctly. If the point (x, y) lies at the centre of a fringe, then $M(x, y)$ will be the integer fringe number, whereas if (x, y) lies anywhere between the centres of two bounding fringes $M(x, y)$ will be an interpolated value between the two fringe numbers. Either the dark or bright fringes may be numbered consecutively, provided that $\Delta M = 1$ between a corresponding type of fringe. For more accuracy, each bright fringe could be given an integer value and each dark fringe between given a half-integer value, although this procedure would double the work of the analysis.

The digital analysis of any interferogram involves determining $M(x, y)$ at any desired location on the picture. This procedure may be broken into three basic parts as follows.

2.1 Assignment of Fringe Numbers

The fringes over the entire interferogram are initially numbered relative to each other as correctly as possible. When beginning this process on any picture, the number assigned to the first fringe is completely arbitrary since the actual order of interference is unknown. As mentioned, however, once a particular fringe has been given a number, all other fringes must be numbered correctly, relative to it in order that a constant difference k (unknown) be maintained over the entire interferogram between the selected fringe numbers and the actual orders of interference. Each interferogram will have its own value of k which can be easily handled in the subsequent analysis.

Figure 5(a) is an example of a no-flow interferogram taken with uniform conditions and hence uniform refractive index in the test section. Consecutive numbering of the dark fringes was done in a straightforward manner as shown, beginning at the entirely arbitrary value of 21. The assignment of fringe numbers for any no-flow picture is usually quite routine, unless optical imperfections are severe.

Figure 5(b) is the subsequent flow interferogram in which an ionizing shock wave in argon is travelling through the test section from right to left as it diffracts around an expansion corner. (It may be compared with Fig. 1(a) where vertical fringes were used to reveal different flow details.) It is important to point out that the number assigned to the first fringe in this picture is again completely arbitrary, and need have no relationship whatsoever to the no-flow interferogram. To emphasize this point, the fringe numbers have been purposely chosen different from the no-flow picture even in the pre-shock region. It is advantageous, however, to number both pictures in the same direction. The necessary criterion is only that the relative numbering between fringes on a particular interferogram be correct. In this case, some care must be taken in identifying and numbering the fringes near the wall and through the shock wave. There are more complex flows for which, in certain regions, the correct numbers may be very difficult to ascertain, and intuition or experience is necessary. However, it should be mentioned that a mistake in numbering of even one fringe will usually give physically unrealistic results. Hence, the correct integer values may become obvious from the results, and the interferogram may be easily re-analysed with the proper fringe numbers.

2.2 Digital Storage of Fringe Coordinates

The locations of each fringe of interest over the interferogram are then recorded using a suitable 'digitizer'. A digitizer consists basically of a 'tablet' on which a chart or picture may be secured, and a travelling cursor which may be moved at will over the tablet. The location of the cursor at any point on the tablet is displayed continuously by a digital read-out of the x and y coordinates (usually in one hundredths of an inch) with respect to the axes and origin of the tablet. These (x, y)-coordinates may be recorded through some interface such as digital tape, either continuously at a desired rate of points per second, or point by point, by depressing a 'log' button with the cursor at the desired location.

The interferogram is placed on the digitizing tablet, with its (x, y)-coordinate system oriented correctly with respect to the (x, y)-axes of the tablet. This is generally accomplished by using known surfaces or crosswire locations on the interferogram as a reference (see Figs. 1, 5, and 8(a)) to ensure the correct positioning and provide the necessary correspondence between the digitizer coordinate system and that used on the interferogram. After alignment has been established, the centre of each fringe is then traced over the interferogram using the digital cursor. When recording in the point mode, the cursor is moved in steps along the fringe, depressing the log button at each step to record the (x, y)-coordinate. In the continuous mode, the log button is held depressed and the recording of coordinates is done automatically at a preselected number per second as the cursor is moved continuously along the fringe. The two recording modes are used interchangeably with continuous recording in regions where the fringe is smooth, and a more careful point by point recording where rapid variations occur. In either mode, the recorded points must be sufficiently close for the subsequent analysis such that the fringe location between any two points can be accurately given by a joining straight line. Consequently, when digitizing has been completed, a sufficient number of points will have been digitized (recorded) to accurately define the location of each fringe anywhere over the interferogram.

An example of the results of this procedure is shown in Fig. 6. In this case, the dark fringes, digitized from the interferogram in Fig. 5(b) have been replotted using an IBM 1627 Calcomp Digital Plotter connected with an IBM 1130 computing system. Each fringe, of course is actually described by a number of recorded, discrete points as shown at the top of the figure for a particular fringe number. In the full plot, the plotter pen has merely been left down as it travelled from point to point along each fringe. As can be seen, it is an accurate representation of the interferogram, and the data are now in digital form suitable for analysis.

2.3 Determination of $M(x, y)$

The value of M at any desired location (x, y) is necessary if eq. (2.6) is to be used to find the refractive index at that point. Since many points across the interferogram have

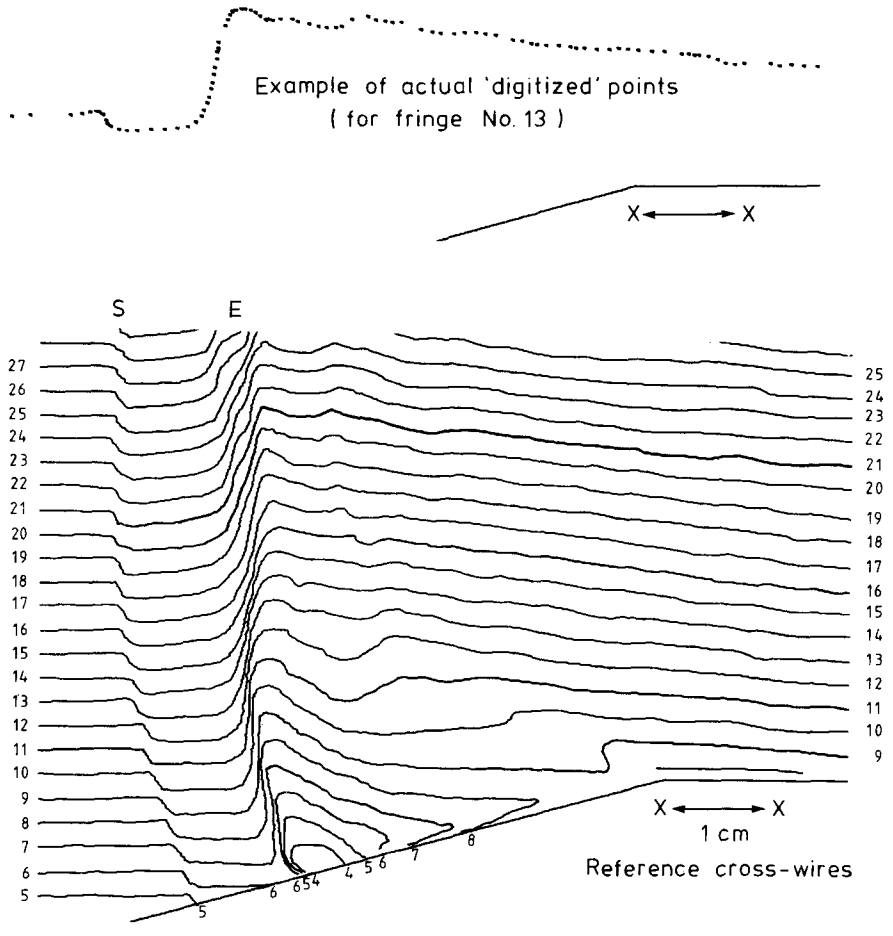

Fig. 6. Digitized version of the interferogram shown in Fig. 5(b)

been recorded by the digitizing procedure at which integer values of M (fringe numbers) are known, a two-dimensional interpolation scheme would seem appropriate, if it were not somewhat lengthy, in finding M at other positions. However, if the position of *each fringe* can be determined accurately, even between the discrete points by linear interpolation (straight-line segments) as specified above, the problem remains only in finding $M(x, y)$ at *off-fringe* locations. Restating this, since lines can be defined from the digitizing procedure along which M is known, all that remains is to determine M at positions not on the lines. This is accomplished in the following manner.

The interferogram is divided into a grid of constant '*argument*' lines, as closely spaced as desired and generally perpendicular to the average direction of the no-flow fringes. The most convenient choice of argument lines (although not a necessity) for data handling are lines along which one coordinate remains constant. For example, with basically horizontal fringes as in Fig. 6, a grid of lines of constant x is generated as shown in Fig. 7(a). For vertical fringes, a grid of lines of constant y would be most suitable. From the digitized data, the intersection points of any fringes with an argument line can be found. Thus, for each argument line, a plot may be made of fringe number versus the coordinate of intersection. The quantity M may then be found at any coordinate along the argument line by a one-dimensional interpolation. As a result, to find M at any location (x, y), the correct argument line passing through the point is chosen, along which discrete values of M are known, and a one-dimensional interpolation is done along the line to find M at this point.

The procedure is demonstrated in Figs. 7(a) and (b) where the grid consists of lines x_i = constant. For each argument line a plot may be made of the variation of fringe number M with y as shown in Fig. 7(b). An interpolation of chosen order may be done to determine M at any specific value of y. This process is handled easily by a computer and may be performed quickly and often.

With a method available for determining $M(x, y)$ as desired from any interferogram, the use of eq. (2.6) will now be examined in more detail. After the interferometer has been suitably aligned with the desired number and spacing of virtual fringes, a no-flow interferogram is taken where the refractive index in the test section has a known and uniform value,

$$n(x, y) = n_0 = \text{constant}$$

Then

$$n_0 L + \tau_0^*(x, y) = \pm M_0(x, y)\lambda + k_0\lambda \qquad (2.7)$$

where again, the subscript 0 denotes the no-flow picture. Although n_0 is known and $M_0(x, y)$ can be determined from the interferogram, k_0, the constant difference between the fringe numbering and the real orders of interference is not known.

For the subsequent interferogram taken of the flow under study, eq. (2.6) will be simply restated:

$$n(x, y)L + \tau^*(x, y) = \pm M(x, y)\lambda + k\lambda$$

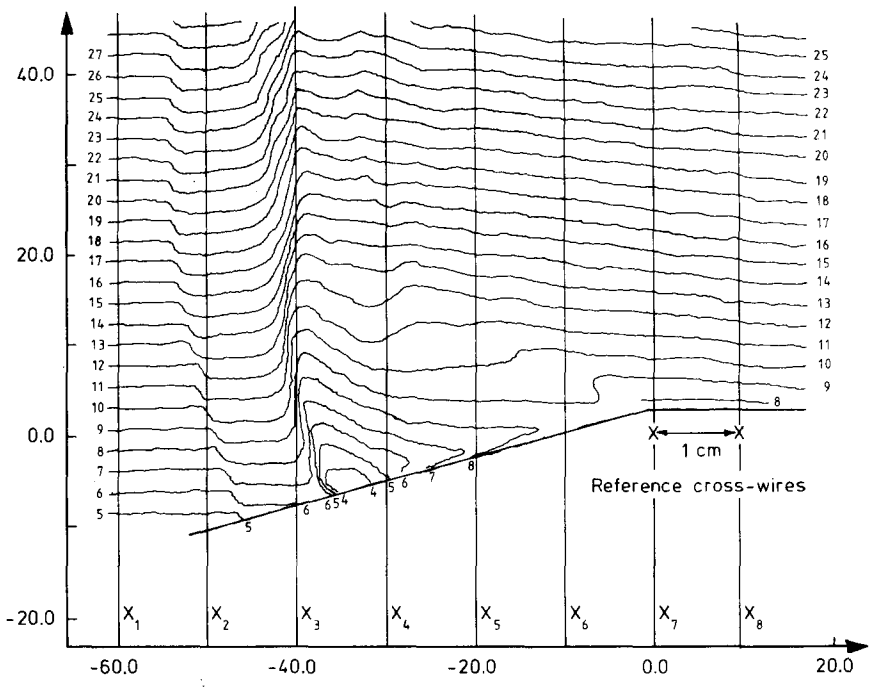

Fig. 7(a). Superposition of argument lines x_i = constant on digitized interferograms. (Note in an actual analysis the grid lines would be much more closely spaced.)

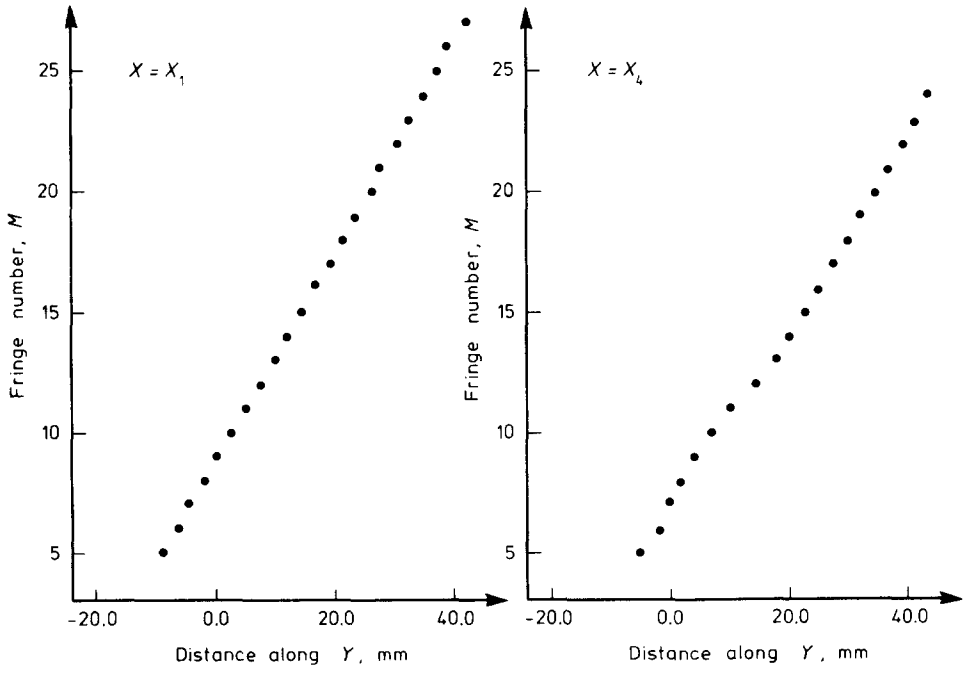

Fig. 7(b). Plots of fringe number M versus fringe position y along argument lines x_i

It is advantageous that the fringe numbering in the flow picture be *in the same direction* as in the no-flow picture, such that the *same sign* holds in both expressions. Subtracting,

$$[n(x, y) - n_0]L + [\tau^*(x, y) - \tau_0^*(x, y)] = \pm[M(x, y) - M_0(x, y)]\lambda + (k - k_0)\lambda \quad (2.8)$$

If no changes have taken place outside the test section during the time when the two interferograms are taken, then $\tau^*(x, y) = \tau_0^*(x, y)$. Moreover, since n_0 is known, and $M(x, y)$ and $M_0(x, y)$ may be measured from the respective interferograms, it is then possible to determine the refractive index in the flow $n(x, y)$, to within the constant, $(k - k_0)$, that is,

$$[n(x, y) - n_0]L = \pm[M(x, y) - M_0(x, y)]\lambda + (k - k_0)\lambda \quad (2.9)$$

If the difference between the chosen fringe numbering and the actual orders of interference happens to be the same in both pictures, then $k = k_0$, and the calculations may be made directly. If not, it *is* known that $(k - k_0)$ must be an *integer*, and it is not difficult in most cases to

find its value from the results since an incorrect choice usually gives unrealistic answers.

However, it is found from practical experience that the assumption of no change in optical path lengths outside the test section between the no-flow and flow interferograms is often incorrect. This usually arises from the inability to control the outside conditions absolutely. Small temperature changes (and hence density) and minute physical movements of the optical components, caused either thermally or otherwise, are difficult to avoid. Because of this, a stronger method is often used which requires that a *reference point* exist somewhere on the flow interferogram at which the refractive index is known. The use of this reference point can at least accommodate *uniform* changes in $\tau^*(x, y)$ between no-flow and flow pictures and eliminates the necessity of choosing the correct value for $(k - k_0)$.

Denoting the coordinates of this reference point as (x_r, y_r), eq. (2.8) must be satisfied at this *particular* location since it is valid for any point on the interferograms.

$$[n(x_r, y_r) - n_0]L + [\tau^*(x_r, y_r) - \tau_0^*(x_r, y_r)] = \pm[M(x_r, y_r) - M_0(x_r, y_r)]\lambda + (k - k_0)\lambda$$

Subtracting this expression from the general eq. (2.8) for all points

$$[n(x, y) - n(x_r, y_r)]L + [\tau^*(x, y) - \tau_0^*(x, y)] - [\tau^*(x_r, y_r) - \tau_0^*(x_r, y_r)] = \pm\{[M(x, y) - M_0(x, y)] - [M(x_r, y_r) - M_0(x_r, y_r)]\}\lambda \quad (2.10)$$

If the changes which take place in $\tau^*(x, y)$ during the time the no-flow and flow pictures are taken are uniform for all (x, y), then

$$\tau^*(x, y) - \tau_0^*(x, y) = \tau^*(x_r, y_r) - \tau_0^*(x_r, y_r)$$

(It should be noted here that it is almost impossible to account for changes which might take place outside the test section which vary across the field of view.) Equation (2.10) then reduces to:

$$[n(x, y) - n(x_r, y_r)]\frac{L}{\lambda} = [M(x, y) - M_0(x, y)] - [M(x_r, y_r) - M_0(x_r, y_r)] \quad (2.11)$$

Therefore, using some reference point (x_r, y_r):

(a) $n(x_r, y_r)$ must be known, but
(b) $k - k_0$ need not be known,
(c) n_0 need not be known.

The term $M(x_r, y_r) - M_0(x_r, y_r)$ is a particular value determined from the interferograms. It not only accounts for the refractive index change in the test section at the particular point (x_r, y_r), but also for:

(a) the fringe numbering difference between the no-flow and flow pictures, and
(b) any uniform changes occurring outside the test section during the time the two pictures are taken.

This is easily seen if the reference point can be chosen in a region where conditions in the test section have not changed between the no-flow and flow pictures, as in the region ahead of the shock wave in Fig. 5(b). Then, any non-zero value of $M(x_r, y_r) - M_0(x_r, y_r)$ *must* be due either to the choice of fringe numbering made in each picture, or to changes outside the test section.

The right-hand side of eq. (2.11) is termed the fringe shift S which compares the observed change in interference at the point (x, y) between the no-flow and flow interferograms to that at a reference point (x_r, y_r).

$$S(x, y) \equiv \pm\{[M(x, y) - M_0(x, y)] - [M(x_r, y_r) - M_0(x_r, y_r)]\} \quad (2.12)$$

As discussed previously, the choice of sign depends on the initial virtual fringe adjustment of the interferometer. If the fringe numbers have been arbitrarily chosen to increase in the same direction as the actual orders of interference increase, the plus sign holds, whereas, if the numbering were done in the opposite direction, the minus sign must be used. If the incorrect choice of sign is made, all fringe shift values will be opposite in sign from reality, and the calculated refractive index will then vary from the reference value in the reverse manner. Often, negative values of $n(x, y)$ result, easily identifying the mistake. In almost all cases, there is some region in the picture where it is *known* that the density and hence refractive index either increases or decreases, such as through a shock wave, compression wave, expansion wave, contact surface, slipstream, and boundary layer. Consequently, the correct sign, which holds over the entire interferogram, can be easily confirmed or corrected from a brief look at results, and presents no problem in the analysis.

In summary, the usual fringe shift equation for interferometry may be written from eq. (2.12) as:

$$S(x, y) = \frac{L}{\lambda}[n(x, y) - n(x_r, y_r)] \quad (2.13)$$

where

$$S(x, y) = \pm\{[M(x, y) - M_0(x, y)] - [M(x_r, y_r) - M_0(x_r, y_r)]\}$$

Using a digital analysis technique, M_0 and M may be determined from the respective no-flow and flow interferograms at any location (x, y), (including (x_r, y_r) thereby allowing a calculation of S. Therefore, knowing L, λ, and $n(x_r, y_r)$ enables a final determination of refractive index, n, at any location (x, y).

3 PERFORMANCE AND RESULTS

The method of evaluating interferograms discussed in the foregoing was applied to some complex flow-fields such as ionizing shock structures **(9)**, **(10)** ionizing boundary layers **(11)**, **(12)** and non-stationary oblique shock-wave reflections **(13)**, **(14)**. Very satisfactory to good agreement was obtained by Glass *et al.* **(9)**, **(10)** and Liu *et al.* **(11)**, **(12)** who compared the results concerning the total and electron number densities with their analytical predictions that they obtained using sophisticated numerical methods. Very good agreement was obtained in references **(13)** and **(14)** and it is believed that order

and insight has been brought to this old and complex problem.

As illustrations of the effectiveness of the present method of evaluating interferograms, some typical results from the above investigations are discussed. Figure 8(a) shows a representative shock wave in krypton. The interferogram was taken in our 10 cm × 18 cm Hypervelocity Shock Tube at 6943 Å using a 23-cm diameter field of view Mach–Zehnder interferometer equipped with a dual-frequency giant-pulse ruby laser. (The interferogram at 3471·5 Å is not shown as it is not as sensitive to electron number density and visually does not provide any new details.) The shock wave is moving from right to left. The abrupt change in the fringes at the translational shock front S is readily seen. The slow production of electrons through atom-atom collisions is indicated by the gradual decrease in the fringe shift. A sudden fringe shift occurs as an avalanche of electrons is produced by electron-atom collisions at the electron cascade front E, where the maximum electron number density is achieved. Subsequent damped oscillations can be seen in the quasi-equilibrium region after the electron cascade front. The fringes rise as the electron number density decreases due to radiative recombination.

The foregoing method of evaluating interferograms was used to obtain the actual variations of the plasma density (ρ), electron number density (n_e), and degree of ionization (χ) across the shock wave shown in Fig. 8(a). These experimental profiles as well as the analytical predictions are shown in Figs. 8(b) and (c). It is seen that the agreement between experiment and analysis is very good. Further details can be found in references (**9**), (**10**), (**11**), and (**12**). The interaction of a nonstationary planar shock wave (I) with a compression corner of 10° is shown in Fig. 9(a). (A detailed sketch is given in Fig. 9(c).) This particular reflection is known as double-Mach reflection. Two three-shock confluences (triple points T and T_1) consisting of three shock waves and one slipstream each are clearly seen.

The density field in the form of constant density contours (isopycnics) associated with this reflection is shown in Fig. 9(b). The isopycnics numbers (m) and the corresponding density values (ρ/ρ_0) are tabulated. The inaccuracy in ρ/ρ_0 for this case is $\Delta\rho/\rho_0 = 0{\cdot}125$ and it is fixed for a given interferogram. The density distribution along the wedge corner associated with this double-Mach reflection is shown in Fig. 9(c). Here also, the inaccuracy in measuring ρ is $0{\cdot}125\rho_0$. A detailed discussion of the maximum absolute possible errors associated with the total densities and electron number densities as measured from the interferograms using the present method of evaluation can be found in (**15**).

The average time for digitizing the four interferograms (two 'flow' and two 'no-flow' pictures) for a given experiment is about two hours. Subsequently, about four to six hours are needed for corrections and final storing on a magnetic computer disc. Once the above is done the total density, electron-number density, and degree of ionization profiles along straight lines at any desired directions (like those shown in Figs. 8(b), 8(c), and 9(c)) can be plotted within minutes. Note that the same results as those shown in Figs. 8(b), 8(c), 9(b), and 9(c) from the corresponding interferograms (Figs. 8(a) and 9(a), respectively) would require at least a couple of days using conventional methods of evaluating interferograms. The accuracy in this case also would be much poorer.

4 DISCUSSIONS AND CONCLUSIONS

A new computerized method for evaluating complex flow interferograms was presented. The present method has the following advantages over previous techniques:

(1) It can easily handle complex-flow fields.
(2) It can account for the changes in the optical path length that occur outside the test section during the time interval taken to record the 'no-flow' and 'flow' interferograms.
(3) Once the interferograms are digitized, corrected, and stored on a computer disc, the total density,

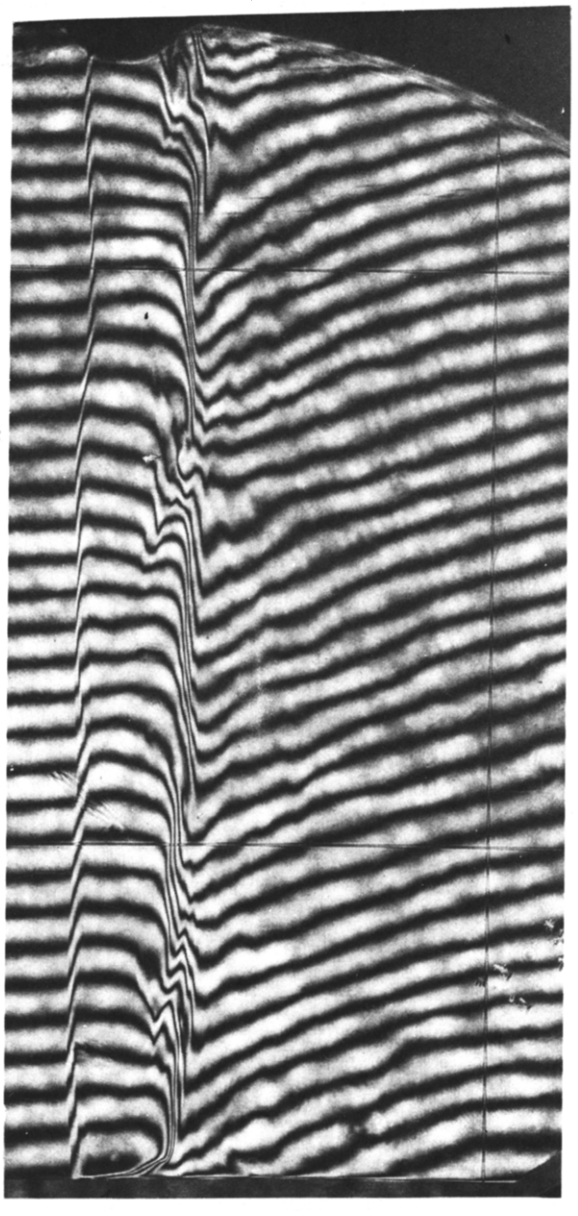

Fig. 8(a). Shock structure in ionizing krypton, over entire shock tube height of 18 cm. S—translational shock front, E—equilibrium ionization (electron cascade front). SE—ionization relaxation distance: $P_0 = 5{\cdot}15$ torr, $T_0 = 296{\cdot}2$ K, $\rho_0 = 2{\cdot}34 \times 10^{-5}$ g/cm^3, $M_s = 15{\cdot}05$. Equilibrium conditions (at point E): $p_E = 1685$ torr, $T_E = 11641$ K, $\rho_E = 1{\cdot}71 \times 10^{-4}$ g/cm^3, $n_e = 1{\cdot}68 \times 10^{17}$/cm, $\chi_E = 13{\cdot}6$ percent. (One vertical and two horizontal reference cross-wires are also shown.)

electron-number density, and degree of ionization profiles can be obtained along any predetermined line within several minutes.

One outstanding problem, the solution of which would reduce the evaluation even further, is to develop a totally automated computerized method of evaluating interferograms rather than the semi-computerized (hand digitized) method presented here. Undoubtedly, such a solution would evolve if more experimenters made more use of interferometry for investigating complex flows. However, the correct assignment of fringe number over the field of view, to represent correctly the interference order, would probably still be done manually.

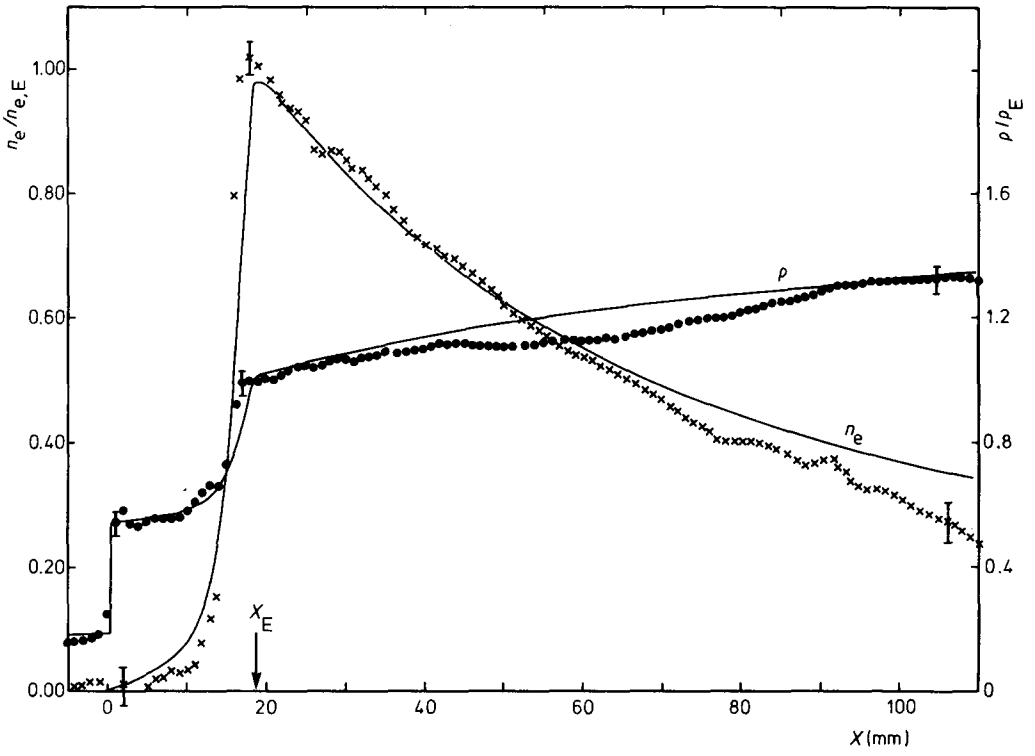

Fig. 8(b). Variation of plasma density and electron number density with distance for shock wave shown in Fig. 8(a)

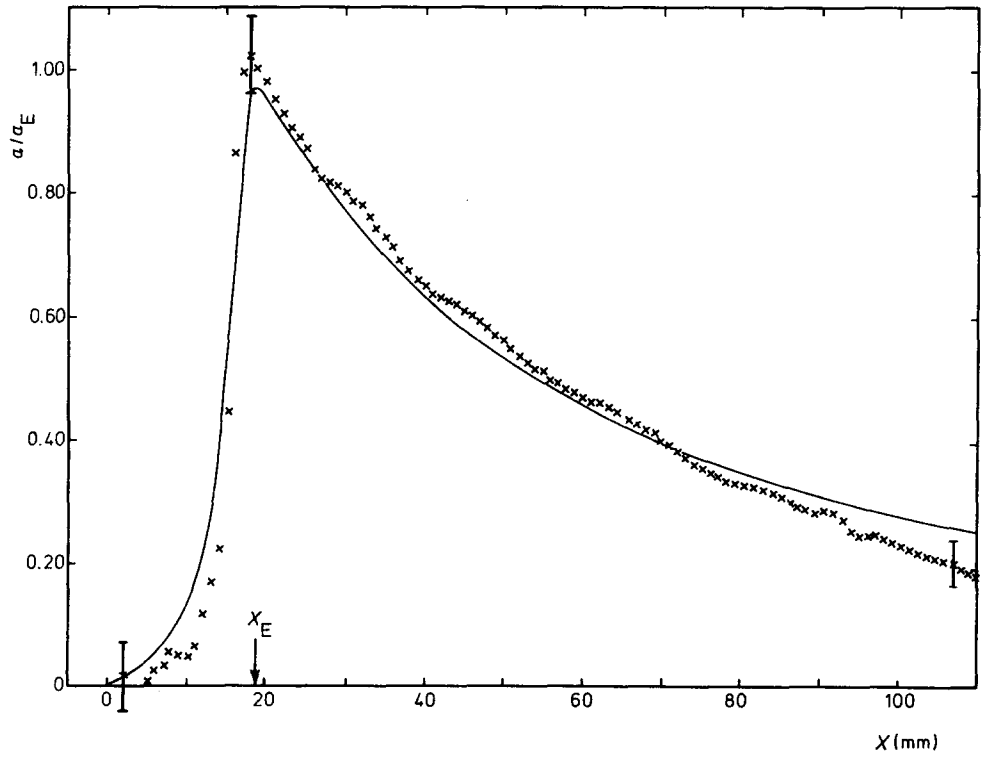

Fig. 8(c). Variation of degree of ionization with distance for shock wave shown in Fig. 8(a)

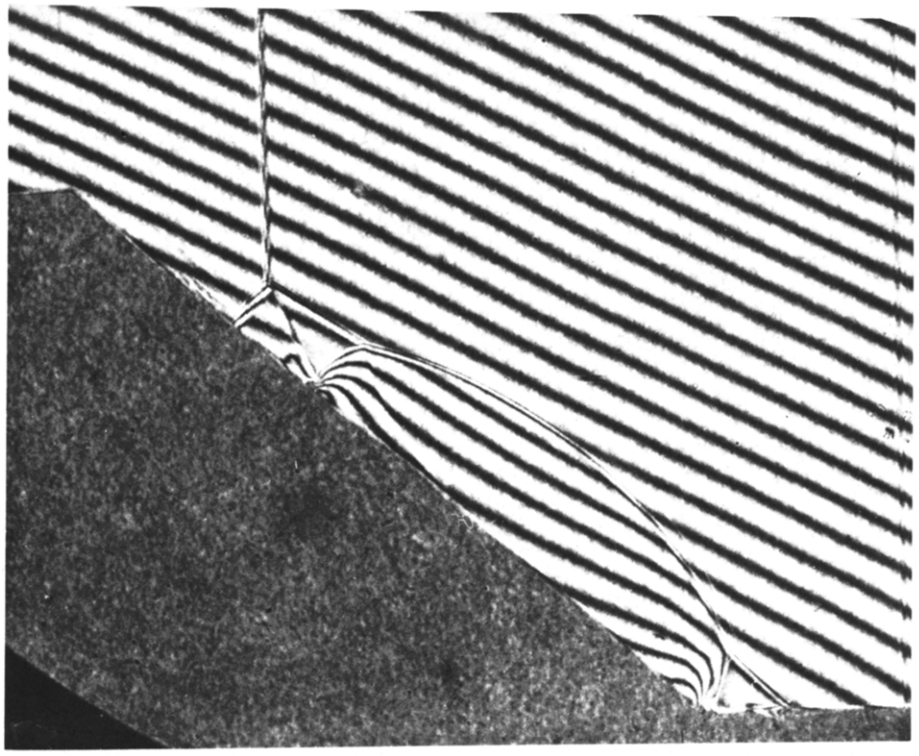

Fig. 9(a). Interferogram of a non-stationary double-Mach reflection in nitrogen $M_s = 3{\cdot}76$, $\theta_w = 40°$, $P_0 = 15{\cdot}34$ torr, $T_0 = 297{\cdot}4$ K

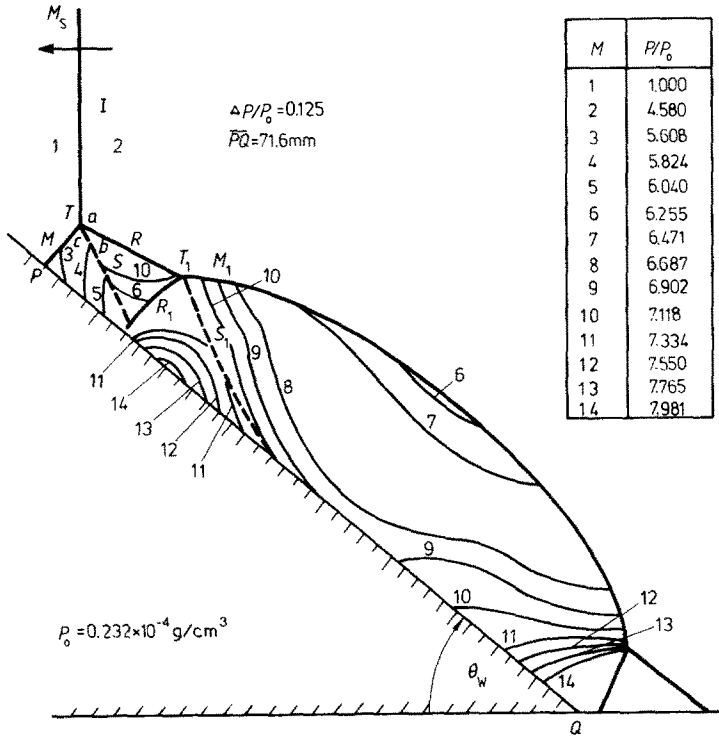

M	P/P_0
1	1.000
2	4.580
3	5.608
4	5.824
5	6.040
6	6.255
7	6.471
8	6.687
9	6.902
10	7.118
11	7.334
12	7.550
13	7.765
14	7.981

Fig. 9(b). Actual flow isopycnics corresponding to the non-stationary oblique shock-wave diffraction shown in (a). I—incident shock wave, R and R_1—first and second reflected shock waves, S and S_1—first and second slipstreams, T and T_1—first and second triple points, M and M_1—first and second Mach stems. Calculated density ratios in vibrational equilibrium: point 1—4·586, b—7·908, c—5·669 and 4·383, 7·286, 5·086, respectively for a perfect diatomic gas

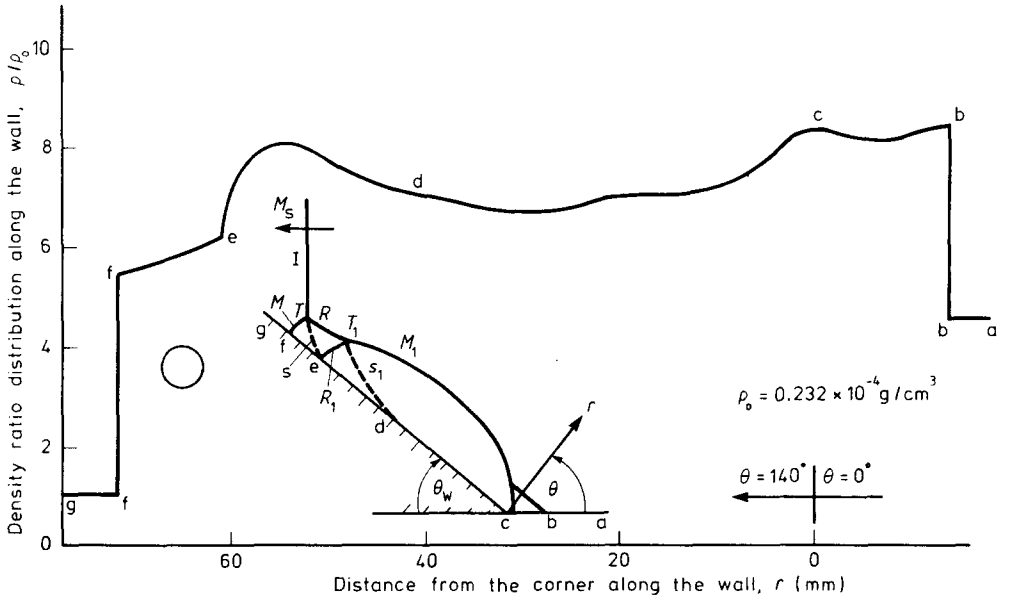

Fig. 9(c). Interferometric density ratio distribution along the wall for the diffraction shown in Fig. 9(a)

ACKNOWLEDGEMENT

The financial assistance received from the US Air Force under Grant AF-AFOSR-77-3303 and from the National Research Council of Canada are gratefully acknowledged.

REFERENCES

(1) LADENBURG, R., and BERSHADER, D. 'Physical Measurements in Gas Dynamics and Combustion', 1954, Article A3, Princeton University Press

(2) ANDERSON, J. H. B., OSBORNE, P. J. K., and GLASS, I. I. 'Gladstone-Dale Constants for Oxygen Atom and Molecule', *Phys. of Fluids* 1967, **10** (8), 1848

(3) IGRA, O., and GLASS, I. I. 'Corner Expansion Flow of Ionizing Argon', *Can. J. Phys.* 1971, **49** (21), 2671–2679

(4) ZEHNDER, L. 'Ein neuer Interferenzrefraktor', *Z. Instrumentenkunde* 1891, **11**, 275–285

(5) MACH, L. 'Über einen Interferenzrefraktor', *Z. Instrumentenk.* 1892, **12**, 89–93

(6) KINDER, W. 'Theorie des Mach–Zehnder-Interferometers und Beschreibung eines Gerates mit Einspiegeleinstellung', *Optik* 1946, **1**, 413–448

(7) HALL, J. G. 'The Design and Performance of a 9-inch Plate Mach–Zehnder Interferometer', 1954, UTIAS Report No. 27

(8) GOLDSTEIN, R. J. *Measurements in Heat Transfer* 1976, Chapter 5 (McGraw-Hill)

(9) GLASS, I. I., and LIU, W. S. 'Effects of Hydrogen Impurities on Shock Structure and Stability in Ionizing Monatomic Gases. Part 1: Argon', *J. Fluid Mech.* 1978, **84**, Part 1, 55–77

(10) GLASS, I. I., LIU, W. S., and TANG, F. C. 'Effects of Hydrogen Impurities on Shock Structure and Stability in Ionizing Monatomic Gases, Part 2: Krypton', *Can. J. Phys.* 1977, **55** (14), 1269–1279

(11) LIU, W. S., WHITTEN, B. T., and GLASS, I. I. 'Ionizing Boundary Layers: 1. Quasi-Steady Flat-Plate Laminar Boundary-Layer Flows', *J. Fluid Mech.* 1978, **87**, Part 4, 609–640

(12) LIU, W. S., and GLASS, I. I. 'Ionizing Argon Boundary Layers: 2. Shock Tube Sidewall Boundary-Layer Flows', *J. Fluid Mech.* 1979, **91**, Part 4, 641–668

(13) BEN-DOR, G., and GLASS, I. I. 'Domains and Boundaries of Nonstationary Oblique Shock-Wave Reflections. Part 1. Diatomic Gas', *J. Fluid Mech.* (to be published, 1979)

(14) BEN-DOR, G., and GLASS, I. I. 'Nonstationary Oblique Shock-Wave Reflections. Actual Isopycnics and Numerical Experiments', *AIAA Journal* 1978, **16** (11), 1146–1153

(15) BEN-DOR, G., and WHITTEN, B. T. 'Interferometric Techniques and Data Evaluation Methods for the UTIAS 10 cm × 18 cm Hypervelocity Shock Tube', UTIAS Tech. Note No. 208, 1979

(16) JONES, A. R., SCHWAR, M. J. R., and WEINBERG, F. J. 'Generalizing Variable Shear Interferometry for the Study of Stationary and Moving Refractive Index Fields with the Use of Laser Light', *Proc. Roy. Soc.* Lond. 1971, **A322**, 116–135